33ND INTERNATIONAL COSMIC RAY CONFERENCE, RIO DE JANEIRO 2013
THE ASTROPARTICLE PHYSICS CONFERENCE

Long term variation of the solar diurnal anisotropy of galactic cosmic rays over four solar activity cycles

K. MUNAKATA[1], M. KOZAI[1], A. ISHIZAKI[1], T. NAKAJIMA[1], C. KATO[1], S. YASUE[1], AND J. KÓTA[2]

[1]*Physics Department, Shinshu University, Matsumoto, Nagano 390-8621, Japan.*
[2]*Lunar and Planetary Laboratory, University of Arizona, Tucson, AZ 85721-0092, USA.*

kmuna00@shinshu-u.ac.jp

Abstract: We analyze the three dimensional (3D) anisotropy of the galactic cosmic ray (GCR) intensity observed with a multi-directional muon detector over four solar activity cycles between 1971 and 2011 and compare them with the anisotropy seen by neutron monitors (NMs) to examine the rigidity dependence of the anisotropy. We clearly see the phase of the free-space diurnal anisotropy shifting toward earlier hours around solar activity minima in A>0 epochs from ∼18 hr local solar time in A<0 epochs. The magnitude of the phase-shift is much larger in the muon data than in the NM data. In particular, we find that the anisotropy component perpendicular to the magnetic field, (after correction for the solar wind convection and the Compton-Getting effect due to Earth's orbital motion around the Sun) is significantly larger in the muon data than that in NM data, while the parallel components in two data sets are quite similar to each other. This energy dependence of the perpendicular anisotropy, which is seemingly due to the harder energy spectrum of the drift streaming than the diffusion in this energy region, naturally explains the larger phase-shift observed in muon data. We also find a clear correlation of the magnitude of the parallel anisotropy with the solar wind velocity which varies without any clear 11-year or 22-year periodicity.

Keywords: Diurnal anisotropy, Heliospheric modulation of galactic cosmic rays, Solar cycle variation of the modulation parameters.

1 Introduction

The Galactic Cosmic Ray (GCR) intensity measured at the Earth changes with various time scales. The solar cycle variation of the modulation parameters alters the spatial distribution of GCR density in the heliosphere and causes the long-term variation of the diurnal anisotropy of the GCR intensity at the Earth, such as the 22-year variation of the anisotropy in which the phase (or local time of maximum) of the diurnal anisotropy shifts towards earlier hours around every A>0 solar minima [1]. By analyzing the 3D anisotropy observed with neutron monitors (NMs) in 1968-1988, Chen & Bieber (1993) revealed that the observed phase-shift of the diurnal anisotropy is due to the decrease of the diffusion streaming parallel to the interplanetary magnetic field (IMF) around A>0 solar minima [2]. Drift models predict smaller radial gradients (G_r) for the A>0 epoch if the parallel and perpendicular diffusion coefficients are the same in both A>0 and A<0 cycles [3]. Finding a significant 11-year variation but no clear 22-year variation in the observed G_r, however, Chen & Bieber (1993) suggested that the smaller paralell streaming in the A>0 cycle was caused by the smaller scattering meanfreepath (m.f.p.) of GCRs due to magnetic helicity effects in the turbulent IMF [2, 4]. Bieber & Chen (1991) also reported that the phase variation increases with particle rigidity, but no physical cause has been suggested for this rigidity dependence so far [5, 6].

In this paper, we follow the analysis by Chen & Bieber (1993) and analyze the long-term variation of the anisotropy observed over the last four solar cycles by NMs monitoring ∼10 GV primary GCRs. In addition to the NM data, we also analyze the anisotropy observed by a multi-directional muon detector responding to ∼50 GV GCRs and examine the energy dependence of the anisotropy.

2 Data analysis and results

The 3D anisotropy of GCRs consists of two components, one lying in the ecliptic plane and the other pointing normal to the ecliptic plane. The ecliptic component is observed as the diurnal anisotropy of GCR intensity, while the normal component is observed as the north-south (NS) anisotropy. We deduce the ecliptic component from the diurnal anisotropy observed by the Newark NM in 1971-2011, while we derive the NS anisotropy (ξ_{NS}) from the difference between intensities recorded at northern and southern polar NMs, Thule and McMurdo NMs, same as [2]. We follow analyses described in [2, 4, 5], except that we use in this paper the Stanford Mean Magnetic Field [7] for identifying the daily mean IMF sector polarity, instead of the omnitape IMF data and the daily sector polarity by Svalgaard used in [2]. We also analyze the monthly mean diurnal variation of the pressure corrected hourly muon rate recorded in each of 17 directional channels of Nagoya multidirectional muon detector [8]. By using the coupling coefficients calculated for each directional channel, we deduce the free-space harmonic vector best fit to all of 17 monthly mean diurnal variations [9]. For the analysis of diurnal anisotropy observed with the multidirectional muon detector, readers can refer to [10].

For deducing the free-space harmonic vector (corrected for the geomagnetic deflection of GCR's orbit and the detector's viewing latitude) from the observed diurnal vector, we use the coupling coefficient calculated by assuming a rigidity independent spectrum with the upper limiting

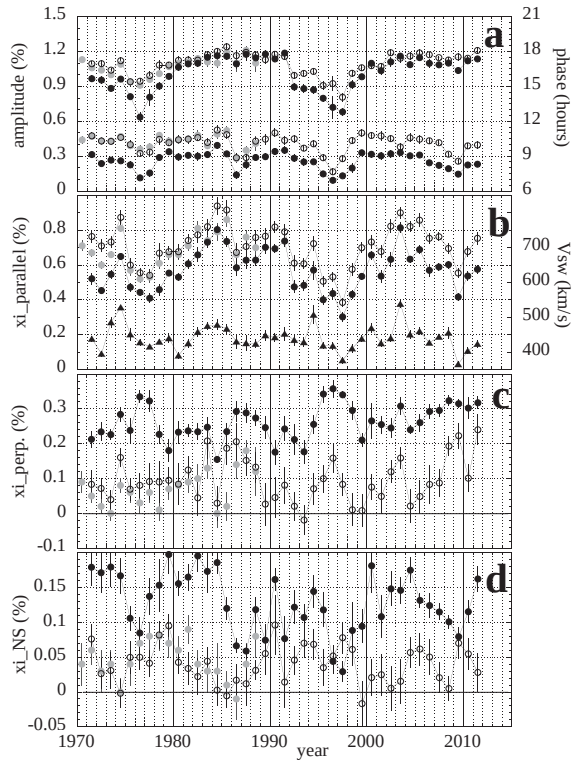

Figure 1: Temporal variation of 3D anisotropy. From the top, each panel displays, as functions of year on the horizontal axis, (a) the amplitude (lower curves on the left vertical axis) and phase (upper curves on the right axis) of the space harmonic vector of the diurnal anisotropy, (b) the parallel anisotropy $\xi_{\parallel}$ (upper curves on the left vertical axis), (c) the perpendicular anisotropy $\xi_{\perp}$ and (d) the NS anisotropy ξ_{NS}. In all panels, open circles represent results derived from our analyses of NM data, while solid circles represents results from Nagoya muon data. For reference, gray solid circles in each panel show results reported in [2]. Solid triangles in panel (b) display the solar wind velocity V_{SW} (lower curve on the right axis). In each panel, yearly mean value and its error are deduced from the average and dispersion of 12 monthly mean values.

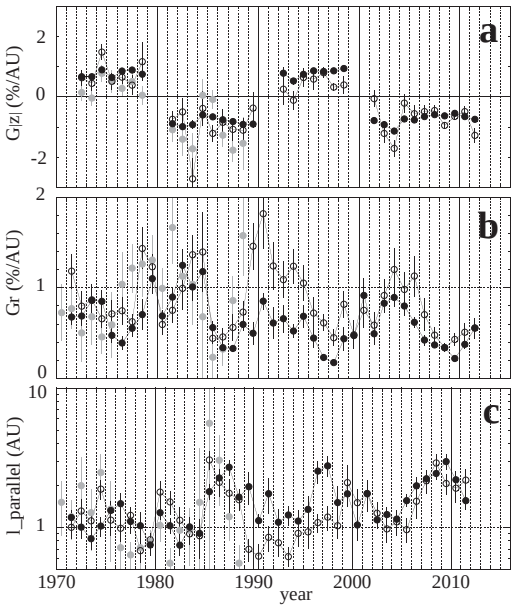

Figure 2: Temporal variations of modulation parameters. From the top, each panel displays, (a) bidirectional latitudinal density gradient ($G_{|z|}$), (b) radial density gradient (G_r) and (c) parallel m.f.p. ($\lambda_{\parallel}$), as functions of year on the horizontal axis. These parameters are deduced from $\xi_{\parallel}$, $\xi_{\perp}$ and ξ_{NS} in figure 1. Note that the vertical axis of panel (c) is logarithmic. Open and solid circles in each panel represent results obtained from the analyses of NM and Nagoya muon data in this paper, respectively, while gray solid circles display results reported in [2]. Errors in panel (c) is propagated from errors of $\xi_{\parallel}$ and G_r used to calculate $\lambda_{\parallel}$. In panel (a) for $G_{|z|}$, we omitted data in years (1971, 1979, 1980, 1991, 1992, 1999, 2000) when a solar magnetic polarity reversal was in progress [15].

rigidity (P_u) set at 100 GV, for both the NM and muon detector data. This rigidity spectrum is same as one assumed in [2].

We subtract from the free-space harmonic vector the Compton-Getting anisotropy arising from the Earth's orbital motion around the Sun and the solar wind convection anisotropy calculated by using the omnitape solar wind velocity [11]. We then obtain the anisotropy components parallel ($\xi_{\parallel}$) and perpendicular ($\xi_{\perp}$) to the magnetic field referring to the omnitape IMF data. The yearly mean harmonic vector and its error are deduced from the average and dispersion of 12 monthly mean vectors, respectively.

For deducing the NS anisotropy (ξ_{NS}) from the observation with Nagoya muon detector, we use the difference ($(GG^T - GG^A)/2$) between muon rates in the GG-component in the Toward (GG^T) and Away (GG^A) IMF sectors. The GG component is a difference combination between intensities recorded in the north- and south-viewing channels and has long been used as a good measure of the NS anisotropy [12]. In this paper, we use the GG-component, for the first time, to analyze the long-term variation of the NS anisotropy. By using the coupling coefficient for the GG component, we derive the monthly mean NS anisotropy in space from $(GG^T - GG^A)/2$ and obtain the yearly mean and its error from the average and dispersion of 12 monthly mean values, respectively.

Figure 1a displays temporal variations of the amplitude (lower curves) and phase (upper curves) of the yearly mean harmonic vector in space, before subtracting the Compton-Getting and solar wind convection anisotropies. Clearly seen in this figure is the phase shifting toward earlier hours in 1976 and 1997 around A>0 solar minima. The magnitude of this phase shift is about ∼3 hours in NM data (open circles), while it is almost double (∼6 hours) in muon data (solid circles), suggesting the rigidity dependence of the anisotropy. The amplitude of the diurnal anisotropy is smaller (larger) around the solar minimum (maximum) period. The clear 22-year variation also seen in $\xi_{\parallel}$ in figure 1b (upper curves) indicates that this component anisotropy is responsible for the phase variation in figure 1a. No such clear signature of 22-year variation is seen in neither $\xi_{\perp}$ nor ξ_{NS} displayed in figures 1c and 1d, respectively.

We also note the following features in this figure. First, there is a close correlation seen in the variations of $\xi_{\parallel}$ by NM and muon detector (open and solid circles in figure 1b,

respectively), while no such clear correlation is seen between variations of $\xi_\perp$ or ξ_{NS} by NM and muon detector in figures 1c and 1d. Second, there is a notable positive correlation seen in figure 1b between the solar wind velocity (V_{SW}) (solid triangles) and $\xi_\parallel$ by NM and muon detector (open and solid circles), producing peaks, for instance, in $\xi_\parallel$ in 1974, 1994 and 2003, when the fast solar wind from the coronal hole is observed at the Earth. Similar correlation with V_{SW} is also seen in $\xi_\parallel$ by [2] (gray solid circles). There is no clear 22-year or 11-year variations are seen in V_{SW}.

Third, we particularly note that the magnitudes of $\xi_\perp$ and ξ_{NS} derived from muon data are significantly larger than those from NM data, while the average magnitude of $\xi_\parallel$ is about $\sim$0.6 % and similar in muon and NM data. This indicates that the rigidity spectra of $\xi_\perp$ and ξ_{NS} are significantly harder than the spectrum of $\xi_\parallel$. This harder rigidity spectrum of $\xi_\perp$ than $\xi_\parallel$ is responsible to the larger phase shift in A$>$0 minimum epochs in muon data, as shown in figure 1a.

Figure 2 shows temporal variations of the modulation parameters deduced from $\xi_\parallel$, $\xi_\perp$ and ξ_{NS} in figures 1b-d. For this deduction, we assumed the ratio of the perpendicular m.f.p. ($\lambda_\perp$) to parallel m.f.p. ($\lambda_\parallel$) to be 0.01 and constant [5]. The bidirectional latitudinal density gradient ($G_{|z|}$) in figure 2a is positive (indicating the local minimum of density on the equator) in A$>$0 epoch, while it is negative (indicating the local maximum of density on the equator) in A$<$0 epoch, in accord with the drift model prediction [3]. The radial density gradient (G_r) in figure 2b remains positive throughout the entire period and appears like changing with $\sim$11 year cycle with maxima (minima) in solar maximum (minimum) periods [2, 4, 5]. The average parallel m.f.p. ($\lambda_\parallel$) deduced from the NM data (open circles) in figure 2c seems to be larger during A$<$0 solar minima around 1985 and 2008 than that in A$>$0 solar minima in 1974 and 1994. This is qualitatively consistent with results reported in [2]. In $\lambda_\parallel$ deduced from muon data (solid circles), on the other hand, the 11 year variation is more prominent with maxima in every solar minimum in 1976, 1977, 1997 and 2009.

3 Summary and discussions

We analyzed the long-term variations of the 3D anisotropy of GCR intensity observed by NMs (Newark, Thule and McMurdo) and the Nagoya muon detector in 1971-2011. The free-space harmonic vector of the diurnal anisotropy changes its phase to earlier hours in A$>$0 solar minima from $\sim$18 hr known as the phase of the "corotation" anisotropy, while the amplitude changes in 11-year cycle and becomes minimum in years around the every solar minimum. The magnitude of the phase change is significantly larger in muon data than in NM data indicating the rigidity dependence of the diurnal anisotropy. A clear 22-year variation is seen in the parallel component ($\xi_\parallel$) of the anisotropy confirming the conclusion by [2] that this component is responsible for the phase change of the space harmonic vector.

We find a close correlation between the variations of $\xi_\parallel$ by NM and muon detector, while no such correlation is seen in variations of $\xi_\perp$ and ξ_{NS}. The average magnitude of $\xi_\parallel$ is also similar in muon and NM data, but the average magnitudes of $\xi_\perp$ and ξ_{NS} derived from muon data are two or three times larger than those from NM data, indicating a harder rigidity spectra of $\xi_\perp$ and ξ_{NS} than that of $\xi_\parallel$. We find, for the first time, that this harder rigidity spectrum of $\xi_\perp$ than $\xi_\parallel$ is responsible to the larger phase shift in A$>$0 minimum epochs in muon data. $\xi_\perp$ and ξ_{NS} include contributions from the drift streaming (or diamagnetic drift streaming) added to the perpendicular diffusion streaming, while $\xi_\parallel$ consists of the parallel diffusion alone. It is reasonable, therefore, to expect that the harder spectrum of $\xi_\perp$ and ξ_{NS} is due to the drift streaming [13]. If this is the case, we would need to assume two types of spectrum combined in $\xi_\perp$ and ξ_{NS} to obtain the correct space harmonic vector. Such an analysis will be presented elsewhere. Hall et al. (1997) examined the rigidity dependence of the anisotropy by analyzing NM data together with muon data, but they also assumed a common rigidity spectrum for $\xi_\parallel$, $\xi_\perp$ and ξ_{NS} [14].

The free-space anisotropy deduced from muon data is more sensitive to reducing P_u from 100 GV assumed in this paper, for instance, to 50 GV, than the anisotropy from NM data, because of better response of muon detectors to $\sim$ 50 GV GCRs. Reducing P_u for muon data increases $\xi_\parallel$, but it also increase $\xi_\perp$ and ξ_{NS}, which are already much larger in muon data than those in NM data. The free-space anisotropy from muon data, on the other hand, is insensitive to increasing P_u above 100 GV. Two or three times difference between $\xi_\perp$ and ξ_{NS} deduced from muon and NM data, therefore, cannot be resolved by changing P_u assumed, as long as a common rigidity spectrum is assumed for all $\xi_\parallel$, $\xi_\perp$ and ξ_{NS}.

The 11- and 22-year variations are also seen in the modulation parameters in figure 2. The bidirectional latitudinal density gradient ($G_{|z|}$) in figure 2a is positive (negative) in A$>$0 (A$<$0) epoch in accord with the drift model prediction of the local minimum (maximum) of GCR density on the HCS. The 11-year variation is evident in the radial density gradient (G_r) in figure 2b, while no clear 22-year variation is seen as reported by [4]

The parallel m.f.p. ($\lambda_\parallel$) deduced from NM data (open circles in figure 2c) also shows the 11-year variation, while it looks larger in 1985-1986 and 2008-2009 around A$<$0 minima than in 1974-75 and 1996-1997 around A$>$0 minima. This is qualitatively consistent with Chen & Bieber (1993) who proposed an idea of the 22-year variation of $\lambda_\parallel$ due to the magnetic helicity effect [2]. $\lambda_\parallel$ deduced from muon data (solid circles in figure 2c), on the other hand, looks different showing peaks around every solar minimum including minima in 1975-1976 and 1996-1997 in A$>$0 epochs. It also appears like persistently increasing toward the maximum in 2009 for the last three solar activity cycles. The difference between $\lambda_\parallel$s by NM and muon detectors in 1996-1997 in A$>$0 epoch is due to the difference in G_rs. G_r by muon detector records the minimum value in 1996-1997 (see solid circles in figure 2b), while G_r by NM does not (see open circles in figure 2b). This is possibly due to the rigidity dependence of $\xi_\perp$ and ξ_{NS} different from that of $\xi_\parallel$, which is not correctly taken into account in the present analysis.

We also find a notable positive correlation between $\xi_\parallel$ and V_{SW}. This correlation has not been noted so far, but it is also seen in $\xi_\parallel$ by [2] and is consistent with the convection-diffusion picture in which the fast solar wind convection increases the radial density gradient and enhances the inward diffusion along the IMF. According to our preliminary analysis, the correlation coefficient between V_{SW} and

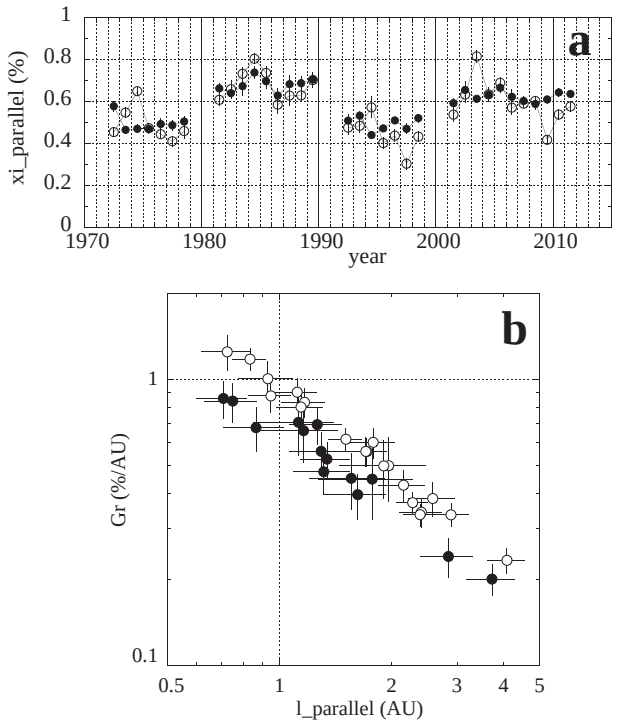

Figure 3: Correction of $\xi_{||}$ for the solar wind effect and correlation between G_r and $\lambda_{||}$ in figure 2. Panel (a) displays temporal variations of $\xi_{||}$ uncorrected (open circles) and corrected (solid circles) for the solar wind effect. In panel (b), G_r on the vertical axis is plotted as a function of $\lambda_{||}$ on the horizontal axis, both in the logarithmic scale. Open and solid circles represent results in A< 0 and A> 0 epochs, respectively. $\xi_{||}$, G_r and $\lambda_{||}$ in this figure are all deduced from the muon data. We excluded from plotting the data in years (1971, 1979, 1980, 1991, 1992, 1999, 2000) when a solar magnetic polarity reversal was in progress [15].

$\xi_{||}$ by muon data in figure 1b exceeds +0.9 and the regression coefficient is about $\sim +0.2$ %/100km/s, indicating that the observed variation of $\xi_{||}$ may contain the solar wind effect which is almost a half of the observed 22-year variation of $\xi_{||}$ in figure 1b. For analyzing the "genuine" 22-year variation of $\xi_{||}$ free from the solar wind effect, therefore, it is necessary to correct the observed $\xi_{||}$ for the solar wind effect. Open and solid circles in figure 3a display $\xi_{||}$s before and after the correction for the solar wind effect. $\xi_{||}$ after the correction (solid circles) remains almost constant over A>0 or A<0 epochs. It looks like stepping up (down) in every A>0 to A<0 (A<0 to A>0) polarity reversal, resembling to $G_{|z|}$ in figure 2a.

Figure 3b finally shows the correlation between G_r and $\lambda_{||}$ which are deduced by using $\xi_{||}$ corrected for the solar wind effect in figure 3a. Open and solid circles display the correlation in A<0 and A>0 epochs, respectively. Similarly to the conclusion by [2], it is possible to attribute the difference between open and solid circles to larger (smaller) $\lambda_{||}$ on the horizontal axis in A<0 (A>0) minimum, resulting in open (closed) circles shifted to the right (left). On the other hand, it is more natural to attribute the difference to larger (smaller) G_r on the vertical axis in A<0 (A>0) epochs, as drift model predicts, resulting in open (closed) circles shifted upward (downward). It is noted that the difference between average G_r in A<0 and A>0 epochs is only $\sim$0.1 %/AU and difficult to detect separately from the 11-year variation with much larger amplitude of $\sim$1 %/AU.

Acknowledgment: This work is supported in part by the joint research program of the Solar-Terrestrial Environment Laboratory (STEL), Nagoya University. The observations with the Nagoya multi-directional muon detector are supported by Nagoya University. Newark neutron monitor of the Bartol Research Institute is supported by NSF grant ATM-0527878. We thank the World Data Center for Cosmic Rays, Solar-Terrestrial Environment Laboratory, Nagoya University, for providing the neutron monitor data analyzed in this paper. Wilcox Solar Observatory data used in this study was obtained via the web site http://wso.stanford.edu at 2013:06:24_22:12:55 PDT courtesy of J.T. Hoeksema. The Wilcox Solar Observatory is currently supported by NASA. JK thanks for the hospitality of the STEL and the Shinshu University supplied during his stay as the visiting professor of the STEL.

References

[1] T. Thambyahpillai and H. Elliot, Nature **171** (1953) 918-920.
[2] J. Chen and J. W. Bieber, The Astrophysical Journal **405** (1993) 375-389.
[3] J. Kóta and J. R. Jokipii, The Astrophysical Journal **265** (1983) 573-581.
[4] J. W. Bieber and M. A. Pomerantz, The Astrophysical Journal **303** (1986) 843-848.
[5] J. W. Bieber and J. Chen, The Astrophysical Journal **372** (1991) 301-313.
[6] S. Y. Oh, Y. Yi and J. W. Bieber, Solar Physics, **262** (2010) 199-212.
[7] http://wso.stanford.edu/meanfld/.
[8] http://www.stelab.nagoya-u.ac.jp/ste-www1/div3/muon/dbtext22.pdf.
[9] K. Fujimoto, et al., Rep.9, Cosmic Ray Res. Lab., Nagoya, Japan (1984).
[10] K. Munakata, et al., Journal of Geophysical Research, **103** (1998) 26851-26857.
[11] http://omniweb.gsfc.nasa.gov/ow.html
[12] M. Laurenza, et al., J. Geophys. Res. **108** (2003) 1069-1075.
[13] J. Minnie, J. W. Bieber, W. H. Matthaeus and R. A. Burger, The Astrophysical Journal **670** (2007) 1149-1158.
[14] D. L. Hall, M. L. Duldig and J. E. Humble, The Astrophysical Journal **482** (1997) 1038-1049.
[15] http://wso.stanford.edu/Polar.html